

Dissecting Multimodal In-Context Learning: Modality Asymmetries and Circuit Dynamics in modern Transformers

Yiran Huang^{1,2}, Karsten Roth³, Quentin Bouliot^{1,2}, Wenjia Xu⁴, Zeynep Akata^{1,2}

¹Technical University of Munich, Munich Center for Machine Learning (MCML), Germany

²Helmholtz Munich, Germany

³Google DeepMind, Switzerland

⁴Beijing University of Posts and Telecommunications, China

Abstract

Transformer-based multimodal large language models often exhibit in-context learning (ICL) abilities. Motivated by this phenomenon, we ask: **how do transformers learn to associate information across modalities from in-context examples?** We investigate this question through controlled experiments on small transformers trained on synthetic classification tasks, enabling precise manipulation of *data statistics* and *model architecture*. We begin by revisiting core principles of unimodal ICL in *modern* transformers. While several prior findings replicate, we find that Rotary Position Embeddings (RoPE) increases the data complexity threshold for ICL. Extending to the multimodal setting reveals a fundamental learning asymmetry: when pretrained on high-diversity data from a primary modality, surprisingly low data complexity in the secondary modality suffices for multimodal ICL to emerge. Mechanistic analysis shows that both settings rely on an induction-style mechanism that copies labels from matching in-context exemplars; multimodal training refines and extends these circuits across modalities. Our findings provide a mechanistic foundation for understanding multimodal ICL in modern transformers and introduce a controlled testbed for future investigation.

1. Introduction

In-context learning (ICL), the ability to perform new tasks from demonstrations without parameter updates (Radford et al., 2019; Brown et al., 2020), has emerged as a core capability of transformer-based large language models (LLMs). Understanding the origins and mechanisms of this capability has become a central focus of transformer research.

For unimodal ICL, progress has been made on both fronts.

On the training side, studies have identified statistical properties of pretraining data, such as burstiness, high class diversity, and skew, that promote ICL over in-weight learning (IWL) (Chan et al., 2022; Singh et al., 2023; Chan et al., 2024; Zucchet et al., 2025). Fundamentally, these mechanisms compete to minimize loss: while IWL relies on memorizing static input-label mappings in parameters, ICL emerges when high data diversity makes such memorization inefficient, forcing the model to rely on context. On the mechanistic side, researchers have traced ICL to specialized *induction circuits*: attention patterns that retrieve contextually relevant examples and copy their associated labels to the query (Olsson et al., 2022; Crosbie & Shutova, 2025; Reddy, 2024). However, these mechanistic insights derive primarily from simplified transformers that lack key architectural components of modern LLMs, such as RoPE.

Recent advances in multimodal large language models (MLLMs) (Alayrac et al., 2022; Abdin et al., 2024; Hui et al., 2024) have extended ICL to interleaved image-text demonstrations, enabling cross-modal reasoning from contextual examples alone. This observation raises a fundamental question about transformer learning:

What enables transformers to perform multimodal ICL, both in terms of training data statistics and mechanisms?

To answer this question, this paper provides a systematic, reverse-engineering account of multimodal ICL in modern transformers. We investigate how statistical principles governing unimodal ICL in simplified transformers (Reddy, 2024) transfer to modern LLM-style architectures, how they extend to multimodal settings, what underlying attention circuits implement multimodal ICL, and how they relate to their unimodal counterparts. To isolate causal factors, we train small but architecturally realistic two-layer transformer models on controllable synthetic classification tasks. This controlled environment allows us to systematically vary data statistics and architectural components while tracking the formation of attention patterns throughout training—an anal-

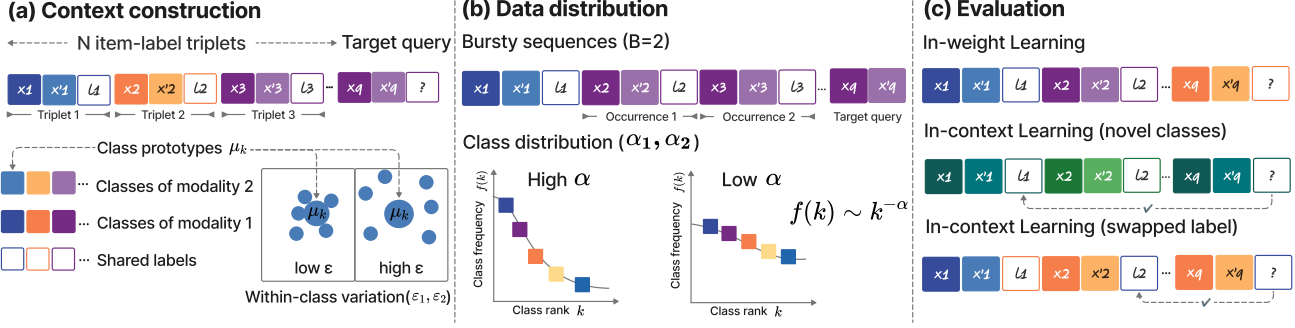


Figure 1. Preliminaries in the multimodal setting. (a) The context consists of N triplets followed by the target query. The paired examples (x_i, x'_i) from two modalities, with a shared label l_i , are generated from Gaussian Mixture Models (GMMs) by controlling within-class variation ε_1 and ε_2 . (b) The distributional properties for the synthetic data. The burstiness B determines how often the class occurs in the context. Class frequencies follow a Zipfian distribution with exponents α_1 and α_2 . (c) Evaluation distinguishes between IWL, where target queries belong to class seen during training while not in the context during evaluation, and ICL, where target queries are novel but in the context. A swapped-label condition further isolates ICL by permuting the labels.

ysis that would be impossible with real-world pretraining corpora, where multiple variables are confounded.

Our investigation yields the following key findings: (1) While the statistical drivers of unimodal ICL in simplified transformers transfer to modern architectures, RoPE raises the data complexity threshold for ICL. Furthermore, scaling up unimodal models favors in-weight memorization over ICL at fixed data complexities (Sec. 3). (2) Multimodal ICL exhibits a strong learning asymmetry. When the model is pretrained on high-diversity data from a primary modality, surprisingly low data complexity in the secondary modality suffices for multimodal ICL to emerge (Sec. 4.1). Consequently, and unlike the unimodal case, scaling consistently improves multimodal ICL. The added capacity is utilized to map the secondary modality to the pre-existing circuit rather than for memorization (Sec. 4.2). (3) Multimodal ICL performance is bottlenecked by the modality alignment; a pretrained encoder is important for achieving this alignment (Sec. 4.3). (4) Beyond synthetic data, we validate our distributional findings and the importance of an encoder on Omniglot (Lake et al., 2019). (5) Mechanistically, induction circuit strength tracks ICL accuracy in both unimodal and multimodal settings. Multimodal training primarily refines the induction head responsible for label matching (Sec. 4.4).

In summary, our contributions are: (1) the first mechanistic account of multimodal ICL in transformers; (2) a controlled testbed for investigating how architectural choices and data statistics shape ICL across modalities; and (3) the discovery of learning asymmetry between modalities and characterization of the underlying circuit dynamics.

2. Preliminaries

Task description. Let \mathcal{X}_1 and \mathcal{X}_2 denote the input spaces of two modalities and let $\mathcal{L} = \{L_1, \dots, L_n\}$ be the shared label set. We feed the model with a context consist-

ing of N labelled exemplars followed by an unlabelled query. In the unimodal setting, we follow Reddy (2024), with context comprising N item-label pairs from a single modality: $x_1, \ell_1, x_2, \ell_2, \dots, x_N, \ell_N, x_q$. Each $x_i \in \mathcal{X}_1$ is an example whose ground-truth label is $\ell_i \in \mathcal{L}$. The model must predict ℓ_q for the query item x_q (see App. A.1). In the multimodal setting, we extend the task by presenting paired exemplars from two modalities: $x_1, x'_1, \ell_1, x_2, x'_2, \ell_2, \dots, x_N, x'_N, \ell_N, x_q, x'_q$. Here $x_i \in \mathcal{X}_1$ and $x'_i \in \mathcal{X}_2$ correspond to the same label ℓ_i (see Fig. 1a). Importantly, at least one exemplar (unimodal) or exemplar pair (multimodal) in the context shares the query’s class, ensuring that ICL is in principle possible.

Synthetic data generation. We consider two modalities and generate data for both modalities from Gaussian Mixture Models (GMMs), allowing for precise control over data properties. For modality $m \in \{1, 2\}$, we sample from a GMM with K_m classes in \mathbb{R}^{D_m} . Class prototypes are $\mu_k \sim \mathcal{N}(0, I_{D_m}/D_m)$, and class instances are generated by:

$$x_i = \frac{\mu_k + \varepsilon_m \eta}{\sqrt{1 + \varepsilon_m^2}}, \quad \text{where} \quad \eta \sim \mathcal{N}(0, I_{D_m}/D_m). \quad (1)$$

The parameter ε_m sets the within-class variability (Figure 1a), with rescaling factor ensuring that $\|x\| \approx 1$. Each modality has K_m classes mapped many-to-one into the shared label set \mathcal{L} . This models fine-grained subclasses collapsing to a common output vocabulary. Each label is also associated with a prototype vector sampled from $\mathcal{N} \sim (0, I_{D_m}/D_m)$. In the multimodal setting, the two generators are dependent. We set the label space $\mathcal{L}_2 \subset \mathcal{L}_1$ to reflect common practice where the decoder generates in the primary modality’s vocabulary (e.g., text), so the secondary modality aligns to that vocabulary rather than expanding it. We use $N = 8, L_1 = 32, L_2 = 16, D_1 = 64, D_2 = 32, \varepsilon_1 = \varepsilon_2 = 0.1$ unless otherwise specified.

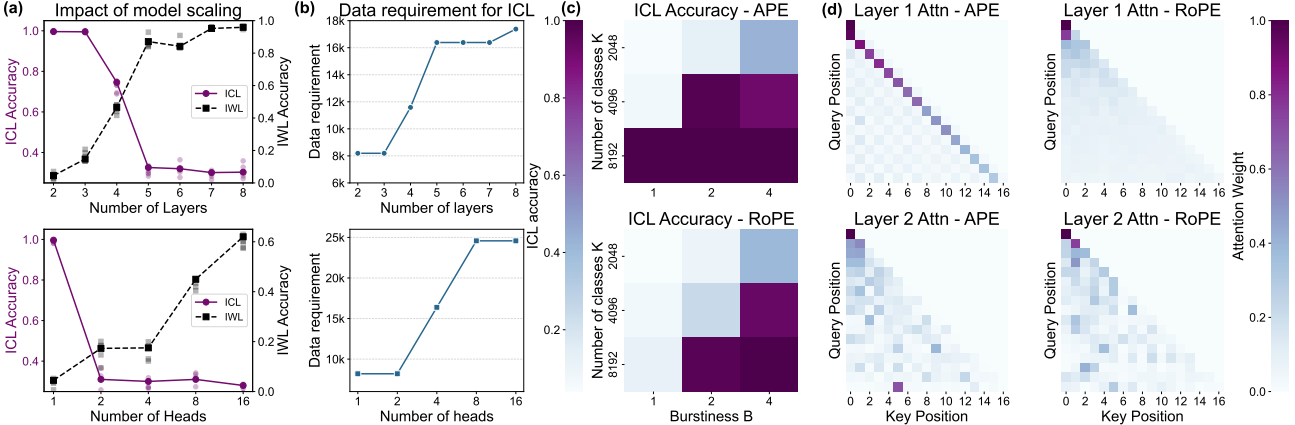


Figure 2. (a) Impact of increasing model layers and attention heads on ICL-IWL tradeoff. Scaling up favours IWL over ICL for five seeds. (b) The data complexity (measured by $K \cdot \sqrt{B}$) required for models of different sizes to achieve the same ICL accuracy (> 0.95). A larger model needs more complex data for a strong ICL capability. (c) Across data regimes, RoPE yields lower ICL accuracy than absolute positional encodings (APE). (d) Attention maps for an example with the correct label at position 5: absolute PE shows clear previous-token and induction heads; with RoPE these patterns are diminished. Here $K = 8192$, $B = 1$, $\alpha = 0$ except when that parameter is varied.

Parameterizing the data distribution. Beyond the intrinsic GMM parameters (D , K , ε), we also control sequence-level statistics. The *burstiness* B (Figure 1b) creates contexts with N/B classes, each appearing B times. This models the multi-shot demonstrations common in real prompts. *Zipfian skew* α (Piantadosi, 2014) parameterizes long-tailed class frequencies $f(k) \sim k^{-\alpha}$ (Figure 1b), determining the balance between frequent and rare concepts.

Training Protocol. We train all models using the SGD optimizer with a batch size of 128. We utilize a learning rate of 1×10^{-3} and a weight decay of 1×10^{-6} . To ensure robust comparisons, all models are trained until convergence.

Evaluation metrics. We explicitly separate two learning mechanisms to avoid misattributing memorization (IWL) to contextual reasoning (ICL). IWL assesses performance on test sequences sampled i.i.d. from the training distribution, measuring knowledge stored in parameters, while ICL assesses performance on sequences with novel classes, forcing reliance on contextual examples rather than memorized associations. As an additional ICL metric, we evaluate the model on sequences in which the context labels are swapped relative to training, invalidating the memorized mapping. We illustrate the evaluation in Figure 1c and App. A.1. To ensure robustness, all reported experiments are averaged over 5 random seeds. For heatmaps, standard deviations are generally < 0.03 unless otherwise noted in the appendix.

3. Establishing Architectural Premises: ICL in Modern Transformers

While previous work (Reddy, 2024) has revealed foundational properties of ICL in attention-only transformers, such as dependency on specific data distribution, it remains un-

clear how these principles operate within modern, LLM-style configurations. Here, we construct a controlled setting to isolate the data-centric and architecture-centric factors that drive ICL, providing premises for the multimodal study. Concretely, we move beyond the attention-only setup and adopt a two-layer transformer decoder architecture incorporating RMSNorm (Zhang & Sennrich, 2019), SiLU (Elfwing et al., 2018), and RoPE (Su et al., 2022), which are components characteristic of contemporary LLMs (Touvron et al., 2023). We systematically vary the statistical properties of the training data and model size, enabling clean attribution of how each factor shapes the emergence of ICL.

3.1. Data statistical principles hold within modern architectures.

All key findings revealed in Reddy (2024); Chan et al. (2022) are reproduced: increasing the number of classes K , burstiness B , or within-class variation ε promotes ICL, while increasing the Zipf exponent α shifts performance toward IWL, with an optimal balance achieved when $\alpha = 1$ (see App. A.2.1). We also recover the ICL-IWL trade-off: settings that strengthen ICL correspondingly diminish IWL, and vice versa. Together, these findings confirm that the core data statistical drivers are architecture-agnostic.

3.2. Model scaling raises the ICL threshold.

We systematically scale up model depth or the number of attention heads and train the model until convergence, using data with the same statistical cues, i.e., same data complexity. We reveal a fundamental tension between model capacity and ICL utilization. Given the same data complexity, larger models tend to favor IWL solutions over ICL ones (Figure 2a). They require substantially stronger statis-

tical cues in training data to achieve the same ICL accuracy (Figure 2b). This requirement grows faster with the number of heads than with the number of layers. We attribute this to how multi-head attention distributes capacity: more heads allow information to be partitioned into specialized subspaces, enabling the item–label memorization. This creates a low-loss shortcut that competes with the ICL solution. Adding layers increases depth but does not create as many independent storage slots for memorization, so the bias toward in-weight learning is weaker. This interpretation aligns with prior observations that induction-style behavior typically emerges in a subset of heads while other heads specialize in memorization (Elhage et al., 2021; Singh et al., 2024). Importantly, *scaling does not eliminate ICL capacity*; it raises the threshold of statistics cues needed for the ICL solution to outcompete memorization.

3.3. RoPE raises the data complexity threshold for ICL.

Switching from absolute positional encodings (APE) to RoPE causes a marked drop in ICL accuracy (Figure 2c). Although RoPE is widely adopted for its strong length generalization, in our setting, this benefit coincides with a consistent degradation of multimodal ICL. Attention visualizations show that the model struggles to form strong previous-token heads with RoPE, and the induction head is also less clear (Figure 2d), which we will investigate in Sec. 4.4. We hypothesize this is because RoPE’s multiplicative rotational structure lacks the discrete, offset-based cues of absolute encodings, making it harder for the model to learn the simple token-copying operations crucial for ICL. For completeness, we also evaluate ALiBi (Press et al., 2021) and Hybrid PE. We provide detailed results including attention circuit analysis with different positional encodings in App. A.2.2, which show that the design of relative positional encodings provides a weaker inductive bias for the simple, offset-based induction circuits. This effect is most pronounced in low-data-complexity regimes, and *sufficiently high data complexity can compensate for this weaker bias*.

Takeaway: Data distributional effects on ICL persist in modern LLM-style transformers. Scaling shifts learning toward in-weight memorization. RoPE further suppresses ICL by disrupting induction circuits.

4. Multimodal In-context Learning

Building on our unimodal ICL baseline, we now investigate the multimodal setting to understand how ICL principles transfer across modalities. We employ a two-stage training process (Figure 3). First, we pretrain a transformer decoder, same as the unimodal setting, on a single primary modality M1. Next, we introduce a secondary modality M2 by adding a simple MLP projector to map M2 features into M1’s em-

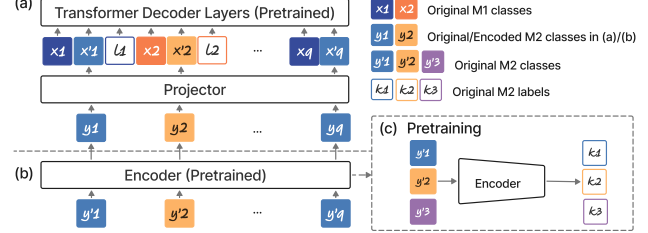


Figure 3. Multimodal setup. (a) Projector-only setup: an MLP projector aligns M2 features to the M1 embedding space. (b) Encoder-augmented setup: a pretrained M2 encoder is stacked before the projector and decoder. (c) Encoder pretraining: the M2 encoder is pretrained on M2-specific classes/labels.

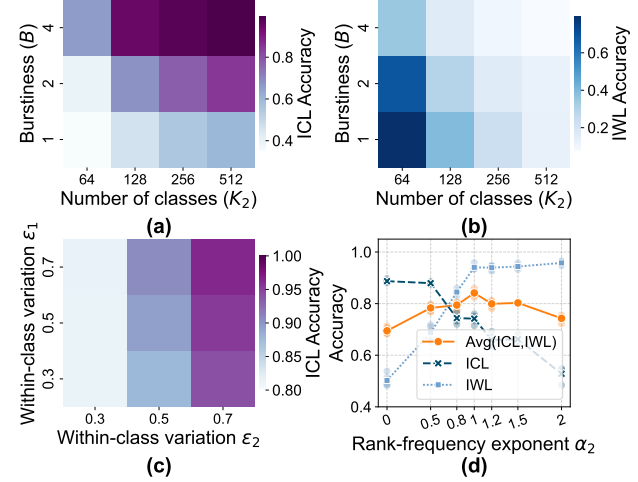


Figure 4. (a) Fixing $K_1 = 8192$, the impact of K_2 and B on ICL performance. When the decoder is pretrained on M1, a significantly lower data complexity for M2 is needed to achieve good ICL. (b) Consistently, IWL decreases with K_2 and B . (c) Raising ϵ_2 benefits ICL markedly more than raising ϵ_1 . (d) Fixing $\alpha_1 = 1$, the ICL–IWL balance is best when $\alpha_2 \approx 1$ for five seeds.

bedding space. We then jointly train it with the pretrained decoder. As an optional extension, we insert a pretrained M2 encoder before the projector to probe representation quality. We use $K_1 = 8192$, $K_2 = 256$, $B = 4$, $\epsilon_1 = \epsilon_2 = 0.1$, $\alpha_1 = \alpha_2 = 0$ unless otherwise specified.

4.1. Data Asymmetries Reveal a Primary and Secondary Role for Modalities.

We examine how the data distributions of two modalities affect ICL. Firstly, the results (Figure 4a) show that increasing the class number and burstiness of M2 increases ICL, similarly to the unimodal setting. Moreover, our experiments reveal a fundamental asymmetry: as shown in Figure 4a, after pretraining the decoder on a high-diversity M1 ($K_1 = 8192$), M2 requires surprisingly little class diversity to achieve comparable ICL; a relatively small $K_2 = 256$ is sufficient. This suggests that M1’s role is to install the

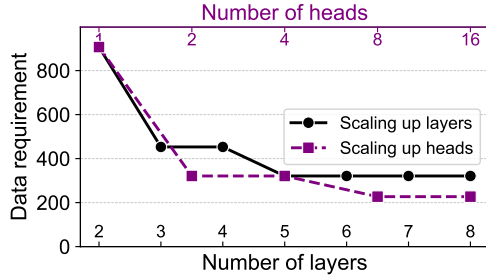


Figure 5. Data requirements (measured by $K_2 \cdot \sqrt{B}$) needed for larger multimodal models to elicit strong ICL. Deeper or wider decoders achieve the same accuracy with lower data requirements.

core ICL capability, while M2’s primary role is simply to provide a distinguishable signal that the projector can map onto the decoder’s pre-existing feature space. Further experiments support this view. While within-class variation ε in both modalities boosts ICL, increasing it for M2 has a much stronger positive effect (Figure 4c). Since M1 is already well-represented from pretraining, higher ε_2 is more critical as it forces the model to learn *a robust and generalizable mapping* for the new modality. Finally, performance is optimized when class-frequency skews (α) match across modalities (Figure 4d): pretraining M1 with $\alpha_1 \approx 1$, the Zipfian skew characteristic of natural-language corpora used to pretrain decoders (Piantadosi, 2014), yields the best multimodal balance when M2 also has $\alpha_2 \approx 1$.

Structural origins of asymmetry. We provide further evidence that the observed primary/secondary hierarchy is a result of the training curriculum. We conducted early-fusion joint training experiments where the model is trained on both modalities from scratch, while strictly maintaining the same interleaved sequence structure (x_i, x'_i, l_i) . We find that removing the pretraining stage reverses the learning asymmetry: the model becomes significantly more sensitive to the data complexity of M2 rather than M1. Detailed results are provided in App. A.3.7. This result confirms that the dominance of M1 in our main analysis is driven by the pretraining phase, which installs the initial ICL circuit. In the absence of this pretraining bias, the model naturally anchors the induction circuit to M2 due to its architectural advantage of being positionally adjacent to the label.

4.2. The Decoder’s Architecture Has Contrasting Effects on Multimodal ICL

Scaling up the decoder favors multimodal ICL. We find that larger models can achieve strong ICL (accuracy $> 95\%$) with significantly lower data complexity requirements (Figure 5). We attribute this to the increased representational bandwidth available in larger models. Since the decoder is initialized with ICL capabilities from the primary modality M1, this added capacity allows it to successfully integrate

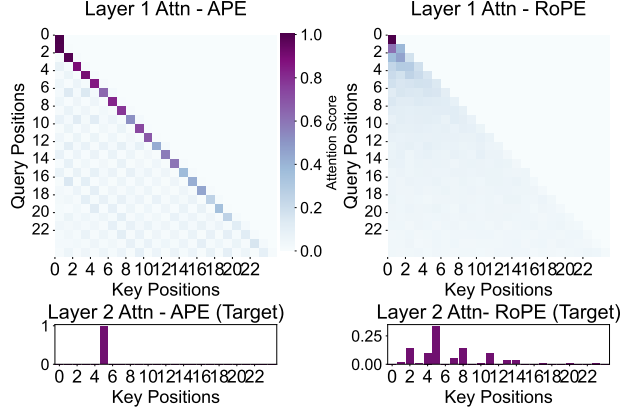


Figure 6. The induction mechanism is preserved in the multimodal setting. Both APE and RoPE exhibit characteristic previous-token copying (Layer 1) and induction spikes at the correct label index 5 (Layer 2). While RoPE blurs the pattern, the persistence of the peak confirms the mechanism transfers to the multimodal setting.

the secondary modality M2 via the projector, thereby enabling effective generalization to the multimodal task.

RoPE continues to raise the data complexity threshold. Consistent with our unimodal findings (Sec. 3.3), RoPE imposes a higher data requirement for ICL emergence in the multimodal setting (see detailed results in App. A.3.1). Interestingly, attention visualizations reveal a crucial mechanistic continuity. As shown in Figure 6, while APE yields sharp previous-token and induction patterns, RoPE exhibits the same mechanistic signature, assigning peak attention to the correct label token despite a more diffuse distribution. This confirms that the core ICL mechanism transfers across modalities, even if RoPE weakens its signal clarity. We provide a detailed quantitative analysis of these circuit dynamics in Sec. 4.4.

4.3. The Role of the Encoder: Cross-Modal Alignment and Feature Quality

While attention mechanisms drive ICL, they can only operate effectively on the representations they receive. Our analysis isolates two critical bottlenecks: cross-modal misalignment and feature discriminability. We demonstrate that the primary role of the encoder is to reshape M2 features to overcome the former, while the quality of the encoder determines the tractability of the latter.

The encoder bridges the misalignment gap. Our initial experiments revealed a consistent drop in ICL accuracy as M2 feature dimensionality increased without any dedicated processing (Figure 7a). This suggests a “misalignment gap”: the projector cannot extract sufficient structure from high-dimensional features to allow the decoder’s induction heads to engage. To address this gap, we introduce a ViT encoder pretrained on M2 data (Figure 3c). We experiment with

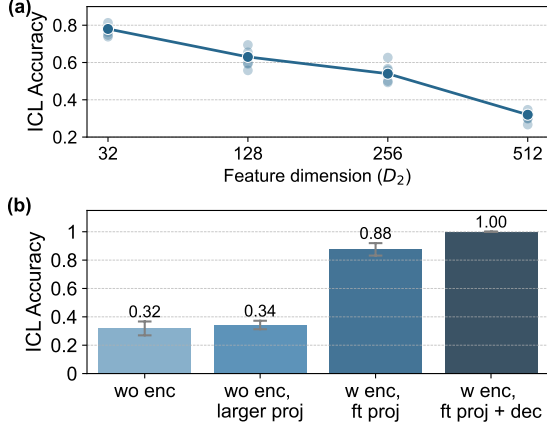


Figure 7. Pretrained encoders enhance multimodal ICL. (a) $D_1 = 64$, increasing M2 feature dimension (D_2) lowers ICL when using only a projector. (b) Fixing $D_2 = 512$, adding a pretrained encoder outperforms a parameter-matched larger projector.

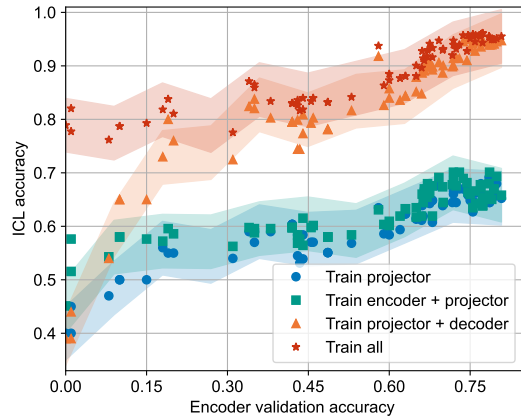


Figure 8. Encoder quality predicts downstream ICL. Multimodal ICL on Omniglot increases with the encoder’s validation accuracy; gains saturate only when the decoder is frozen, while joint training of the decoder continues to yield improvements.

three training strategies: training (1) only the projector, (2) the projector & pretrained decoder, and (3) all the components. Results in Figure 7b indicate that the encoder significantly boosts ICL accuracy across all training regimes. This gain is not merely a function of added capacity; a model with a pretrained encoder consistently outperforms a parameter-matched baseline with a larger projector.

We attribute this improvement explicitly to better cross-modal alignment. Quantitative analysis of the feature space reveals that higher M2 feature dimensions (D_2) degrade the alignment between the two modalities: as D_2 increases from 32 to 512, Centered Kernel Alignment (CKA) drops from 0.16 to 0.07, and Euclidean distance (L_2) increases from 0.95 to 2.15. However, employing the encoder mitigates this misalignment at high dimensions ($D_2 = 512$), increasing

CKA from 0.07 to 0.10 and reducing L_2 from 2.15 to 1.95. Full results are provided in Appendix A.3.2. This suggests the encoder acts as a bridge, compressing the M2 data into a manifold that aligns better with the decoder’s latent space, thereby allowing the decoder to successfully apply its ICL capabilities to the new modality.

Validation on real data reveals the importance of M2 representation quality. While synthetic data offers fine-grained control over distributional properties, it is significantly easier to classify compared to real-world inputs. To further investigate the role of the encoder under more realistic conditions, we extend experiments to Omniglot (Lake et al., 2019) images as M2. Concretely, we first show that all the data distributional findings transfer to real images (App. A.3.3), then train encoders with varying difficulty levels (detailed in App. A.3.4) and thus with different validation accuracies. Afterwards, we measure the impact of these encoders on downstream multimodal ICL.

As shown in Figure 8, encoder validation accuracy strongly predicts multimodal ICL performance. This indicates that the discriminative quality of the input features is critical. A stronger encoder groups similar inputs more tightly, providing a distinct signal that simplifies the projector’s task. By reducing ambiguity in the input space, the encoder allows the projector to more accurately map M2 features to the target M1 embedding space.

Furthermore, joint fine-tuning of the encoder, projector, and decoder yields the highest accuracy, indicating that maximizing ICL requires the co-adaptation of all the components.

Takeaway. With a decoder initialized from unimodal pretraining, strong multimodal ICL is achievable without highly complex data from the second modality. Scaling up the decoder size improves ICL. Additionally, encoders enhance ICL by aligning compressed, discriminative features with the decoder.

4.4. Quantifying ICL Mechanisms

To understand how multimodal ICL emerges mechanistically, we move beyond accuracy curves and analyze the formation of specific attention circuits. Prior work on unimodal simple transformers identified a two-step ICL circuit: an early-layer “previous-token head” copies information, and a later-layer “induction head” uses it to find matching examples and retrieve their labels (Olsson et al., 2022). However, these circuits can be difficult to detect when attention patterns are diffuse, particularly with RoPE. To quantify the circuit dynamics of ICL even when the patterns are not clearly visible, we employ a suite of progress measurements designed to track the formation of key attention patterns.

4.4.1. PROGRESS MEASUREMENTS

Let Attn_m denote the attention matrix at transformer layer m for a sequence of length L_{seq} .

Previous Token Head Strength (PHStrength) measures attention paid by all the tokens to their immediate predecessor. We define:

$$\text{PHStrength}_m^{(1)} = \frac{1}{L_{\text{seq}} - 1} \sum_{i=1}^{L_{\text{seq}}-1} \text{Attn}_m(\text{query}_i \rightarrow \text{key}_{i-1}). \quad (2)$$

In the multimodal interleaving setting, where useful dependencies may shift by an additional offset, we also track attention to the token two positions back: $\text{PHStrength}_m^{(2)}$.

Induction Head Strength (IndStrength) quantifies how strongly the target token attends to the labels of the context examples of the same class.

$$\text{IndStrength}_m = \frac{1}{|\mathcal{P}|} \sum_{j \in \mathcal{P}} \text{Attn}_m(\text{query}_{\text{target}} \rightarrow \text{key}_j), \quad (3)$$

where \mathcal{P} is the set of positions immediately after context examples of the same class as the target.

Target Label Association (TLA) measures total attention the target token paid to all context label positions.

$$\text{TLA}_m = \sum_{j \in \mathcal{Y}} \text{Attn}_m(\text{query}_{\text{target}} \rightarrow \text{key}_j), \quad (4)$$

where \mathcal{Y} is the set of positions of all the labels in the context.

Context-label Accuracy (CLA) measures if the predicted label appeared in the context, indicating reliance on context. Let \hat{y} be the predicted label, $\{y_i\}_{i=0}^N$ the labels of the N context examples, then

$$\text{CLA} = \mathbb{P}(\hat{y} \in \{y_i\}_{i=1}^N). \quad (5)$$

Except for Context Label Accuracy, all metrics are computed separately for each transformer layer.

4.4.2. ICL DYNAMICS: FROM FORMATION TO REFINEMENT

Our analysis reveals a distinct two-stage evolution of the ICL circuit. Unimodal pretraining installs the foundational circuit, while multimodal training primarily refines it to accommodate new modalities.

Correlation analysis reveals a shift in ICL’s primary driver. We compute the Pearson correlation between metrics and ICL accuracy for the runs with varying data statistics for five seeds. The results in Table 1 differ significantly between the two settings. In the unimodal pretraining, $\text{PHStrength}_1^{(1)}$ (previous-token copying) and

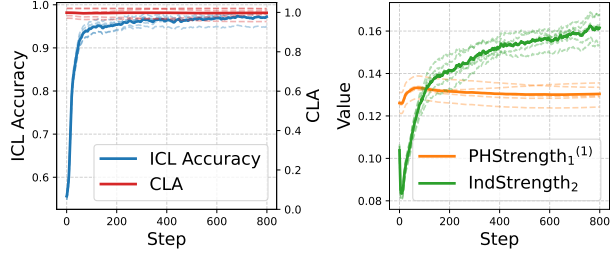


Figure 9. Demonstration of the head dynamics in the multimodal setting for five seeds. While CLA and previous token heads remain stable from the unimodal stage, the refinement of the induction head is the primary driver of accuracy gains.

Table 1. Pearson correlations (ρ) between top progress measurements ($\rho \geq 0.5$) and ICL accuracy. In the unimodal setting, learning foundational mechanisms like previous-token copying and context reliance is dominant. In the multimodal setting, the focus shifts to refining the label-matching induction head.

(a) Unimodal Setting		(b) Multimodal Setting	
Metric	ρ	Metric	ρ
$\text{PHStrength}_1^{(1)}$	0.72	IndStrength_2	0.70
CLA	0.65	$\text{PHStrength}_1^{(1)}$	0.58
IndStrength_2	0.61	TLA_2	0.56
TLA_1	0.59	CLA	0.02

IndStrength_2 (label matching) show the strongest correlation with ICL accuracy. CLA (predicting the label from the context) is also a strong correlate. This confirms that initial ICL development is driven by learning the foundational mechanisms of an induction circuit: learning the “looking back” and “copy” operation.

However, in the multimodal setting, the dynamics shift. We find that IndStrength_2 becomes the strongest correlate of ICL accuracy. Conversely, the correlation for CLA drops to just 0.02. As shown in Figure 9, this is because the model, having already mastered context-reliance during pretraining, maintains a high CLA ceiling throughout the multimodal stage. Crucially, $\text{PHStrength}_1^{(1)}$ remains a strong correlate, while $\text{PHStrength}_1^{(2)}$ shows negligible correlation. This confirms that the model does not alter its fundamental copying mechanism to span two tokens (skipping the M1 token to look at M2 directly); instead, it reuses the same offset-one circuit established during pretraining. This shift suggests that the model reuses the foundational behaviors learned in pretraining and the new bottleneck for performance is applying this circuit to M2. The model must learn to match the M2 query feature to the context examples, and this “matching” skill is precisely what IndStrength_2 quantifies.

To assess whether these mechanisms are sufficient to explain performance, we split all the runs into training /validation sets and train a random-forest regressor to predict ICL accu-

Table 2. A random forest regressor can predict final ICL accuracy (R^2) from our progress measurements in both settings.

Feature Subset	Unimodal	Multimodal
PHStrength ₁ ⁽¹⁾ , IndStrength ₂	0.91 ± 0.02	0.90 ± 0.01
PHStrength ₂ ⁽¹⁾ , TLA ₁ , IndStrength ₂	0.96 ± 0.02	0.96 ± 0.06
All metrics	0.97 ± 0.01	0.98 ± 0.01

Table 3. Effect of Circuit Ablation on multimodal ICL.

Configuration	ICL Accuracy ($\pm \sigma$)
Baseline	0.970 ± 0.025
Knocking out Previous Token Head	0.199 ± 0.005
Knocking out Induction Head	0.062 ± 0.003

racy from the progress measurements. The results in Table 2, demonstrate that the core ICL circuit is highly predictive in both settings. Full analysis see App. A.3.5.

4.4.3. VALIDATING THE MECHANISM

Validating Circuit Necessity. While progress measurements correlate strongly with ICL accuracy, correlation does not imply causation. To validate the mechanistic necessity of these multimodal ICL circuits, we move beyond the correlation analysis and perform targeted causal interventions at inference time. Concretely, we identify the previous token head and induction head (head with max PHStrength₁⁽¹⁾ and IndStrength₂) and knock them out by zeroing the corresponding attention. The results in Table. 3 confirm these circuits are causal drivers of performance.

Cross-Modal Integration. To confirm that this circuit refinement represents genuine cross-modal integration rather than a degenerate reliance on the primary modality, we conduct a modality zeroing ablation at inference time. Zeroing M2 reduces ICL accuracy from $> 96\%$ to 33.6%, proving induction heads depend on M2 features for discrimination. However, zeroing M1 causes a catastrophic drop to 6.3%. These results (App. A.3.6) confirm that M1 provides the structural scaffold; the model cannot perform ICL from M2 alone because the circuit logic remains anchored in the primary modality’s embedding space.

Takeaway. Unimodal pretraining constructs the specific ICL circuits, while multimodal training refines them.

4.4.4. OBSERVATIONS IN MLLMs

As a supplementary check, we examined whether the induction patterns identified in our controlled setting also appear in MLLMs. We evaluate Qwen2.5-VL (3B/7B) (Team, 2025) and IDEFICS (9B/80B) (Laurençon et al., 2023) on the VL-ICL benchmark (Zong et al., 2024) and analyze

attention using our progress measurements (Sec. 4.4) on Qwen2.5-VL. The results show that larger decoder variants (Qwen2.5-VL-7B vs. 3B; IDEFICS-80B vs. 9B) exhibit improved multimodal ICL, and attention analysis on Qwen2.5-VL reveals more pronounced induction-head signatures in the stronger-performing model. We provide detailed results in App. A.4, where stronger previous-token and induction heads coincide with stronger ICL. We emphasize that these observations are not intended as a mechanistic explanation of MLLMs as production systems involve vastly more complex training regimes, data distributions, and architectural choices that confound clean attribution. Rather, the qualitative consistency suggests that the controlled testbed developed here captures principles that may have broader relevance, and provides a foundation for future mechanistic investigation of multimodal ICL at scale.

5. Related Work

Unimodal ICL. First observed as an emergent LLM ability (Brown et al., 2020), ICL has since been studied in NLP and synthetic settings (Min et al., 2022; Akyürek et al., 2022; Wei et al., 2023; Von Oswald et al., 2023; Singh et al., 2023; Dong et al., 2024), with work probing the roles of training data and demonstrations (Chan et al., 2022; Shin et al., 2022; Yadlowsky et al., 2023; An et al., 2023; Liu et al., 2024). Mechanistic studies have focused on induction circuits, first discovered by Elhage et al. (2021) and further investigated across various settings (Olsson et al., 2022; Wang et al., 2023), alongside theoretical interpretations (Xie et al., 2021; Singh et al., 2024). Reddy (2024) explored ICL emergence through both induction circuits and data distributional properties using minimal attention-only transformers, which particularly motivated our work. While these mechanistic analyses typically use simplified architectures that diverge from modern LLMs in key components, we further investigate more realistic structures and extend the analysis to the multimodal setting.

Multimodal ICL. Existing work on multimodal ICL has primarily focused on understanding or improving the behavior of MLLMs. Studies have documented multimodal ICL capabilities in models pretrained on interleaved image–text corpora (Alayrac et al., 2022; Abdin et al., 2024; Hui et al., 2024; Zong et al., 2024). Others have worked on strengthening this behavior (Zhao et al., 2023; Doveh et al., 2024; Yu et al., 2024; Jiang et al., 2025; Jia et al., 2025; Chen et al., 2025b; Huang et al., 2024). Diagnostic work has revealed that apparent multimodal ICL in MLLMs is often largely text-driven (Chen et al., 2025a; Baldassini et al., 2024). Our work differs fundamentally in scope and objective: rather than analyzing MLLMs or using a simplified model as a proxy to explain MLLM behavior, we study multimodal ICL as a phenomenon in transformers in its own right, contribut-

ing to the broader understanding of transformer learning rather than to MLLM interpretability specifically.

6. Conclusion

We uncover a learning asymmetry where the primary modality installs the core ICL circuit, enabling multimodal ICL to emerge with low data complexity in the secondary modality. This explains why scaling consistently improves multimodal ICL: the added capacity is used to map the secondary modality to the pre-existing ICL circuit, unlike the unimodal tendency where capacity shifts toward memorization. Mechanistically, both settings rely on induction heads, though RoPE universally suppresses this capability.

Impact Statement

In this paper, we present a systematic, mechanistic dissection of multimodal in-context learning (ICL) in transformers and introduce a controlled synthetic testbed for isolating the effects of data statistics and model architecture.

Applications: This research primarily impacts the fundamental understanding of transformer architectures. By establishing a rigorous testbed for “dissecting” how transformers learn to associate information across different input streams, we provide researchers with a tool to investigate learning phenomena that are often obscured in large-scale experiments. This testbed can be applied to study other emergent behaviors in transformers beyond ICL.

Implications: The primary implication of this work is improved transparency and interpretability of transformer models. By mapping high-level capabilities—like cross-modal ICL—to specific, quantifiable attention mechanisms (e.g., the refinement of induction heads), we move closer to explaining how these black-box models function. This mechanistic understanding is crucial for diagnosing why models fail or behave unexpectedly.

Initiatives: We encourage the community to utilize our open, low-compute testbed to democratize interpretability research and further probe transformer learning dynamics. Future work could leverage our findings to investigate circuit-level robustness. Additionally, researchers can use this framework to explore architectural designs that inherently favor robust reasoning over memorization, such as optimizing positional encodings to better support induction circuit formation.

References

Abdin, M., Aneja, J., Behl, H., Bubeck, S., Eldan, R., Gunasekar, S., Harrison, M., Hewett, R. J., Javaheripi, M., Kauffmann, P., et al. Phi-4 technical report. *arXiv preprint arXiv:2412.08905*, 2024.

Akyürek, E., Schuurmans, D., Andreas, J., Ma, T., and Zhou, D. What learning algorithm is in-context learning? investigations with linear models. In *The Eleventh International Conference on Learning Representations*, 2022.

Alayrac, J.-B., Donahue, J., Luc, P., Miech, A., Barr, I., Hasson, Y., Lenc, K., Mensch, A., Millican, K., Reynolds, M., et al. Flamingo: a visual language model for few-shot learning. *Advances in neural information processing systems*, 35:23716–23736, 2022.

An, S., Lin, Z., Fu, Q., Chen, B., Zheng, N., Lou, J.-G., and Zhang, D. How do in-context examples affect compositional generalization? In *Proceedings of the 61st Annual Meeting of the Association for Computational Linguistics (Volume 1: Long Papers)*, pp. 11027–11052, 2023.

Baldassini, F. B., Shukor, M., Cord, M., Soulier, L., and Piwowarski, B. What makes multimodal in-context learning work?, 2024. URL <https://arxiv.org/abs/2404.15736>.

Brown, T., Mann, B., Ryder, N., Subbiah, M., Kaplan, J. D., Dhariwal, P., Neelakantan, A., Shyam, P., Sastry, G., Askell, A., et al. Language models are few-shot learners. *Advances in neural information processing systems*, 33: 1877–1901, 2020.

Chan, B., Chen, X., György, A., and Schuurmans, D. Toward understanding in-context vs. in-weight learning. In *The Thirteenth International Conference on Learning Representations*, 2024.

Chan, S., Santoro, A., Lampinen, A., Wang, J., Singh, A., Richemond, P., McClelland, J., and Hill, F. Data distributional properties drive emergent in-context learning in transformers. *Advances in neural information processing systems*, 35:18878–18891, 2022.

Chen, S., Han, Z., He, B., Liu, J., Buckley, M., Qin, Y., Torr, P., Tresp, V., and Gu, J. Can multimodal large language models truly perform multimodal in-context learning? In *2025 IEEE/CVF Winter Conference on Applications of Computer Vision (WACV)*, pp. 6000–6010. IEEE, 2025a.

Chen, S., Liu, J., Han, Z., Xia, Y., Cremers, D., Torr, P., Tresp, V., and Gu, J. True multimodal in-context learning needs attention to the visual context. *arXiv preprint arXiv:2507.15807*, 2025b.

Crosbie, J. and Shutova, E. Induction heads as an essential mechanism for pattern matching in in-context learning. In *Findings of the Association for Computational Linguistics: NAACL 2025*, pp. 5034–5096, 2025.

Dong, Q., Li, L., Dai, D., Zheng, C., Ma, J., Li, R., Xia, H., Xu, J., Wu, Z., Chang, B., et al. A survey on in-context learning. In *Proceedings of the 2024 Conference on Empirical Methods in Natural Language Processing*, pp. 1107–1128, 2024.

Doveh, S., Perek, S., Mirza, M. J., Lin, W., Alfassy, A., Arbelle, A., Ullman, S., and Karlinsky, L. Towards multimodal in-context learning for vision and language models. In *European Conference on Computer Vision*, pp. 250–267. Springer, 2024.

Elfwing, S., Uchibe, E., and Doya, K. Sigmoid-weighted linear units for neural network function approximation in reinforcement learning. *arXiv preprint arXiv:1702.03118*, 2018.

Elhage, N., Nanda, N., Olsson, C., Henighan, T., Joseph, N., Mann, B., Askell, A., Bai, Y., Chen, A., Conerly, T., et al. A mathematical framework for transformer circuits. *Transformer Circuits Thread*, 1(1):12, 2021.

Huang, B., Mitra, C., Arbelle, A., Karlinsky, L., Darrell, T., and Herzig, R. Multimodal task vectors enable many-shot multimodal in-context learning. *Advances in Neural Information Processing Systems*, 37:22124–22153, 2024.

Hui, B., Yang, J., Cui, Z., Yang, J., Liu, D., Zhang, L., Liu, T., Zhang, J., Yu, B., Dang, K., et al. Qwen2. 5-coder technical report. *CoRR*, 2024.

Jia, H., Jiang, C., Xu, H., Ye, W., Dong, M., Yan, M., Zhang, J., Huang, F., and Zhang, S. Symdpo: Boosting in-context learning of large multimodal models with symbol demonstration direct preference optimization. In *Proceedings of the Computer Vision and Pattern Recognition Conference*, pp. 9361–9371, 2025.

Jiang, Y., Fu, J., Hao, C., Hu, X., Peng, Y., Geng, X., and Yang, X. Mimic in-context learning for multimodal tasks. In *Proceedings of the Computer Vision and Pattern Recognition Conference*, pp. 29825–29835, 2025.

Lake, B. M., Salakhutdinov, R., and Tenenbaum, J. B. The omniglot challenge: a 3-year progress report. *Current Opinion in Behavioral Sciences*, 29:97–104, 2019.

Laurençon, H., Saulnier, L., Tronchon, L., Bekman, S., Singh, A., Lozhkov, A., Wang, T., Karamcheti, S., Rush, A., Kiela, D., et al. Obelics: An open web-scale filtered dataset of interleaved image-text documents. *Advances in Neural Information Processing Systems*, 36:71683–71702, 2023.

Liu, N. F., Lin, K., Hewitt, J., Paranjape, A., Bevilacqua, M., Petroni, F., and Liang, P. Lost in the middle: How language models use long contexts. *Transactions of the Association for Computational Linguistics*, 12:157–173, 2024.

Min, S., Lyu, X., Holtzman, A., Artetxe, M., Lewis, M., Hajishirzi, H., and Zettlemoyer, L. Rethinking the role of demonstrations: What makes in-context learning work? In *Proceedings of the 2022 Conference on Empirical Methods in Natural Language Processing*. Association for Computational Linguistics, 2022.

Olsson, C., Elhage, N., Nanda, N., Joseph, N., DasSarma, N., Henighan, T., Mann, B., Askell, A., Bai, Y., Chen, A., et al. In-context learning and induction heads. *CoRR*, 2022.

Piantadosi, S. T. Zipf’s word frequency law in natural language: A critical review and future directions. *Psychonomic bulletin & review*, 21:1112–1130, 2014.

Press, O., Smith, N. A., and Lewis, M. Train short, test long: Attention with linear biases enables input length extrapolation. *arXiv preprint arXiv:2108.12409*, 2021.

Radford, A., Wu, J., Child, R., Luan, D., Amodei, D., Sutskever, I., et al. Language models are unsupervised multitask learners. *OpenAI blog*, 1(8):9, 2019.

Reddy, G. The mechanistic basis of data dependence and abrupt learning in an in-context classification task. In *The Twelfth International Conference on Learning Representations*, 2024. URL <https://openreview.net/forum?id=aN4Jf6Cx69>.

Shin, S., Lee, S. W., Ahn, H., Kim, S., Kim, H. S., Kim, B., Cho, K., Lee, G., Park, W., Ha, J. W., et al. On the effect of pretraining corpora on in-context learning by a large-scale language model. In *2022 Conference of the North American Chapter of the Association for Computational Linguistics: Human Language Technologies, NAACL 2022*, pp. 5168–5186. Association for Computational Linguistics (ACL), 2022.

Singh, A., Chan, S., Moskovitz, T., Grant, E., Saxe, A., and Hill, F. The transient nature of emergent in-context learning in transformers. *Advances in neural information processing systems*, 36:27801–27819, 2023.

Singh, A. K., Moskovitz, T., Hill, F., Chan, S. C., and Saxe, A. M. What needs to go right for an induction head? a mechanistic study of in-context learning circuits and their formation. In *International Conference on Machine Learning*, pp. 45637–45662. PMLR, 2024.

Su, J., Lu, Y., Pan, S., Wen, B., and Zhai, Y. Roformer: Enhanced transformer with rotary position embedding. *arXiv preprint arXiv:2104.09864*, 2022.

Team, Q. Qwen2.5-v1, January 2025. URL <https://qwenlm.github.io/blog/qwen2.5-v1/>.

Touvron, H., Lavril, T., Izacard, G., Martinet, X., Lachaux, M.-A., Lacroix, T., Rozière, B., Goyal, N., Hambro, E., Azhar, F., et al. Llama: Open and efficient foundation language models. *arXiv preprint arXiv:2302.13971*, 2023.

Von Oswald, J., Niklasson, E., Randazzo, E., Sacramento, J., Mordvintsev, A., Zhmoginov, A., and Vladymyrov, M. Transformers learn in-context by gradient descent. In *International Conference on Machine Learning*, pp. 35151–35174. PMLR, 2023.

Wang, L., Li, L., Dai, D., Chen, D., Zhou, H., Meng, F., Zhou, J., and Sun, X. Label words are anchors: An information flow perspective for understanding in-context learning. In *Proceedings of the 2023 Conference on Empirical Methods in Natural Language Processing*, 2023.

Wei, J., Wei, J., Tay, Y., Tran, D., Webson, A., Lu, Y., Chen, X., Liu, H., Huang, D., Zhou, D., et al. Larger language models do in-context learning differently. *arXiv preprint arXiv:2303.03846*, 2023.

Xie, S. M., Raghunathan, A., Liang, P., and Ma, T. An explanation of in-context learning as implicit bayesian inference. In *International Conference on Learning Representations*, 2021.

Yadlowsky, S., Doshi, L., and Tripuraneni, N. Pretraining data mixtures enable narrow model selection capabilities in transformer models. *arXiv preprint arXiv:2311.00871*, 2023.

Yu, K., Zhang, Z., Hu, F., Storks, S., and Chai, J. Eliciting in-context learning in vision-language models for videos through curated data distributional properties. In *Proceedings of the 2024 Conference on Empirical Methods in Natural Language Processing*, pp. 20416–20431, 2024.

Zhang, B. and Sennrich, R. Root mean square layer normalization. In *Advances in neural information processing systems*, volume 32, pp. 1–11, 2019.

Zhao, H., Cai, Z., Si, S., Ma, X., An, K., Chen, L., Liu, Z., Wang, S., Han, W., and Chang, B. Mmicl: Empowering vision-language model with multi-modal in-context learning. In *The Twelfth International Conference on Learning Representations*, 2023.

Zong, Y., Bohdal, O., and Hospedales, T. M. Vl-icl bench: The devil in the details of benchmarking multimodal in-context learning. *CoRR*, 2024.

Zucchet, N., d’Angelo, F., Lampinen, A. K., and Chan, S. C. The emergence of sparse attention: impact of data distribution and benefits of repetition. *arXiv preprint arXiv:2505.17863*, 2025.

A. Appendix

This appendix presents comprehensive methodological details, extended mechanistic analyses, and external validation of the findings reported in the main text. Section A.1 formalizes the experimental framework, detailing the synthetic data generation processes and the evaluation protocols used to distinguish in-context learning (ICL) from in-weights learning (IWL). Section A.2 extends the unimodal analysis, investigating the mechanistic impact of positional encodings (RoPE, ALiBi, APE) and verifying the causal link between attention metrics and model performance via random forest analysis. Section A.3 provides a deep dive into multimodal dynamics: we analyze feature alignment, validate findings on real image data (Omniglot), and conduct critical ablation studies—including modality zeroing and early-fusion joint training—to demonstrate that cross-modal ICL relies on genuine geometric integration rather than degenerate heuristics. Finally, Section A.4 bridges the gap to practice, demonstrating that the mechanistic signatures of induction heads and decoder scaling laws observed in our controlled settings directly translate to production-grade MLLMs such as Qwen2.5-VL and IDEFICS.

A.1. Preliminaries

In the unimodal setting, inputs consist of N labeled tuples followed by a query (Figure 10a). Figure 10b summarizes the synthetic data generation and distributional controls, and Figure 10c details the IWL/ICL evaluation protocol.

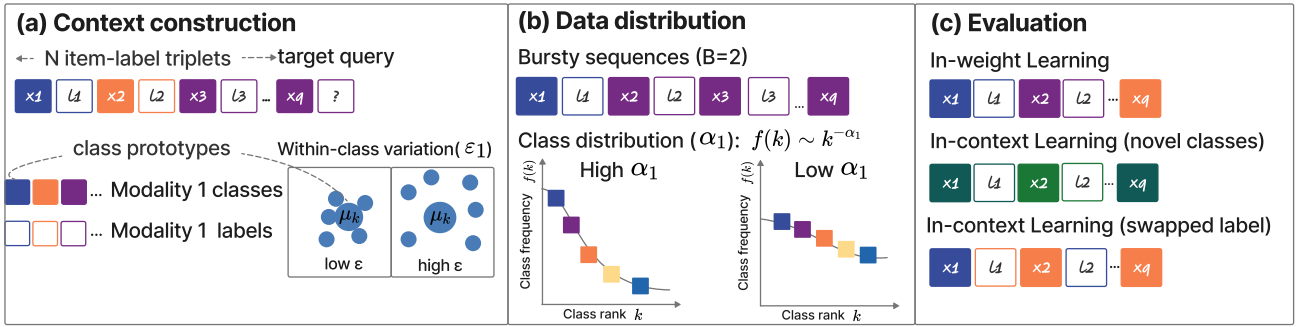


Figure 10. Overview of the preliminaries in the unimodal setting. (a) The context consists of N item-label pairs (x_i, l_i) followed by the target query. K classes are assigned to L labels. (b) The distributional properties for the synthetic data. Class instances are obtained by controlling within-class variation ε . Class frequencies follow a Zipfian distribution with exponent α , and burstiness B determines repeated class occurrences in context. (c) Evaluation distinguishes between in-weight learning, where test items belong to seen classes while not in the context, and in-context learning (ICL), where test classes are in the context but novel. A swapped-label condition further isolates ICL by permuting label assignments during evaluation.

Evaluation metrics. We separate IWL from ICL to avoid conflating memorization with contextual reasoning, following Reddy (2024); Chan et al. (2022). Each test episode is a sequence of N labeled exemplars (context) followed by a query; unless stated, we match training hyperparameters (e.g., N , burstiness B , Zipf exponent α , within-class variation ε). **IWL:** sample both context items and the query i.i.d. from the *training* class distribution with the same priors; the query’s class does not appear in the context examples. **ICL–Novel (primary test):** use novel classes unseen during training, provide labeled exemplars for those classes in the context, and draw the query from the same novel-class set; this measures the ability to infer class–label mappings from context alone. **ICL–Swap (label-swap control):** use training classes but apply a random permutation to context labels at test time and evaluate against the permuted mapping; this invalidates memorized mappings and isolates reliance on context. We report accuracy for IWL, ICL (average of ICL–Novel and ICL–Swap).

A.2. Extended results and analysis in unimodal experiments

A.2.1. UNIMODAL DATA DISTRIBUTIONAL PROPERTIES

As shown in Figure 11, key trends are reproduced. In addition, we notice that while higher within-class noise ε again promotes ICL, we additionally find that it slows convergence, as the model requires more data to form robust associations.

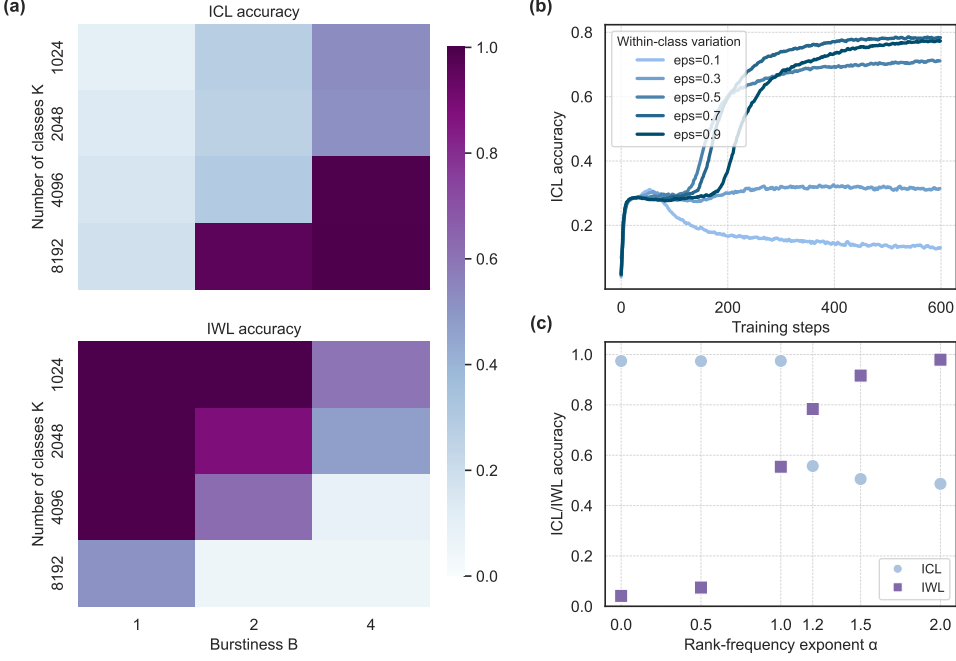


Figure 11. The data distributional findings transfer from the GMM setting. (a) *Number of classes and burstiness.* Larger number of classes K and burstiness B promotes ICL while decreasing IWL. (b) *Within-class variation.* Increasing ϵ promotes ICL. However, it also slows down the emergence of ICL. (c) *Class-distribution skew.* Increasing α improves ICL. When $\alpha = 1$, a balance is achieved between ICL and IWL.

A.2.2. IMPACT OF POSITIONAL ENCODINGS, CONTEXT LENGTH, AND DATA COMPLEXITY

To further investigate the mechanistic impact of positional encodings (PE) discussed in Sec. 3, we conducted a broader analysis comparing **Absolute PE (APE)**, **RoPE**, **ALiBi**, and a **Hybrid (APE + RoPE)** model. We swept two key variables: the context length (N , the number of item-label pairs) and the data complexity (proxied by $K \cdot \sqrt{B}$). The results are shown in Figure 12. First, for a fixed data complexity, ICL accuracy degrades for *all* PE types as the context length (N) increases. This suggests that longer contexts make it more difficult to find the matching exemplar, increasing the difficulty for the ICL circuit (as supported by the decreasing induction circuit strength in Figure 12). Secondly, We observe that ALiBi and RoPE perform similarly, and as argued in Sec. 3, both appear to weaken the formation of the offset-based induction circuits compared to APE. The Hybrid (APE + RoPE) model’s performance lies in between as expected. Third, while APE and Hybrid PE demonstrate stronger ICL performance across most of the tested regimes, it is crucial to note the effect of data complexity. As seen in the high-complexity setting (Figure 12, right), the performance gap narrows significantly. At high complexity and short context lengths (e.g., $N=8$), it is possible for all four PE types to achieve near-perfect ICL accuracy.

These findings show that the design of RoPE and ALiBi provides a weaker inductive bias for the simple, offset-based induction circuits. This effect is most pronounced in low-data-complexity regimes, and *sufficiently high data complexity can compensate for this weaker bias. Importantly, they do not prevent ICL.*

Pearson Correlation. The results in the Table 4a align with the standard induction-circuit picture: PHStrength₁ correlates most with ICL accuracy (previous-token copying), IndStrength₂ ranks highly (label matching), and CLA is also strong, reflecting prediction from context labels. CLA ranks second, indicating that high ICL models tend to predict labels seen in the context. TLA in the first layer shows moderate correlation with ICL accuracy. This suggests that, in addition to the previous token function, the first attention head also contributes to the model learning to predict the labels existing in the context. This is further supported by a Pearson correlation of 0.6 between TLA₁ and CLA, indicating that attention to all context labels in early layers may be a key mechanism behind the model’s ability to select labels from the context.

Random forest prediction. The results in the Table 5 show that the combination of PHStrength₁ and IndStrength₂, which correspond to the two key components of the induction head circuit, achieves an R^2 score of 0.909. This result

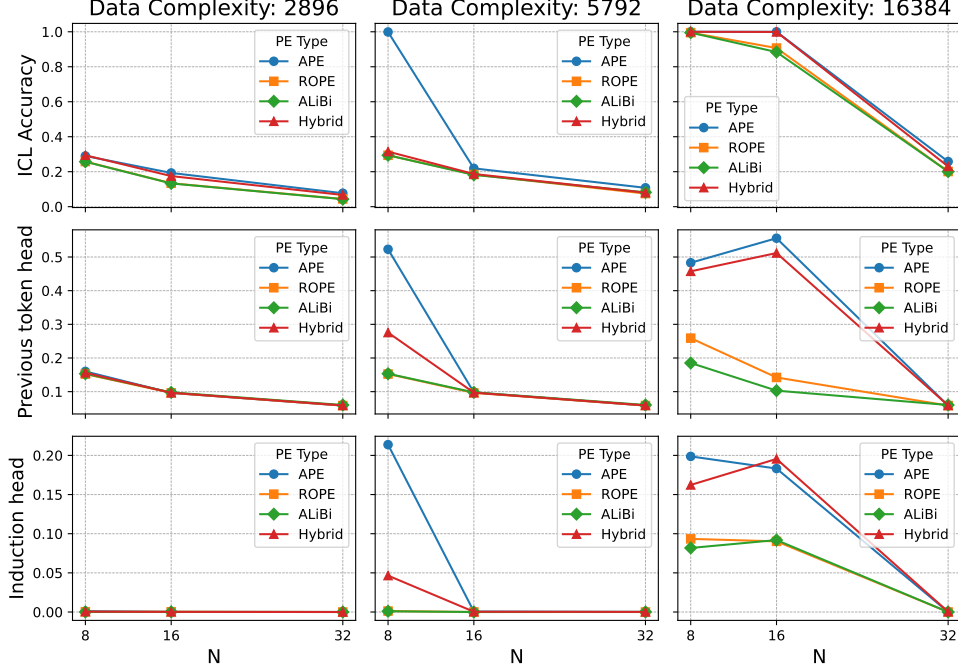


Figure 12. Comparison of the impact of different positional encodings across data complexity and context length on ICL accuracy and the strength of previous token head and induction head. Three key patterns are visible: (1) ICL accuracy degrades for all PE types as context length (N) increases. (2) ALiBi and RoPE cluster together, while APE shows the highest accuracy, with the Hybrid PE performing in between. (3) The performance gap between encodings narrows significantly in the high-complexity regime, where all PEs can achieve near-perfect accuracy at short context lengths.

Table 4. Pearson correlations (ρ) between progress measurements and ICL accuracy. We consider $\rho > 0.5$ strong and $\rho > 0.7$ very strong.

(a) Unimodal setting

Rank	PM	ρ
	PHStrength ₁	0.72
2	CLA	0.65
3	IndStrength ₂	0.61
4	TLA ₁	0.59
5	TLA ₂	0.11
6	IndStrength ₁	0.06
7	PHStrength ₂	-0.10

(b) Multimodal setting

Rank	Metric	ρ
1	IndStrength ₂	0.70
2	PHStrength ₁ ⁽¹⁾	0.58
3	TLA ₂	0.56
4	TLA ₁	0.51
5	PHStrength ₁ ⁽²⁾	0.48
6	PHStrength ₂ ⁽²⁾	0.47
7	IndStrength ₁	0.10
8	CLA	0.02
9	PHStrength ₁ ⁽¹⁾	-0.02

indicates that these two mechanistic metrics alone capture the majority of the variance in ICL accuracy across models trained with varying data distributions and architectures. Adding TLA₁ as a third feature further improves performance to $R^2 = 0.960$. This suggests that the attention to all label positions provides complementary information to the mechanistic induction circuit, likely supporting the model’s broader ability to locate context-relevant labels. This interpretation is reinforced by the earlier finding that TLA₁ correlates moderately with both ICL accuracy and CLA. Using the full set of progress measurements, the regressor achieves an R^2 of 0.974 ± 0.014 , indicating that ICL performance is not only correlated with, but also highly predictable from, internal attention behaviors. These results suggest that attention patterns such as previous-token copying, label-focused attention, and context alignment are not incidental byproducts of learning, but form a reliable, quantifiable foundation for in-context reasoning.

Table 5. Random-forest performance (R^2) for predicting unimodal ICL accuracy from subsets of progress measurements.

Feature subset	R^2 (mean \pm std)
PHStrength ₁ , IndStrength ₂	0.91 \pm 0.02
PHStrength ₁ , TLA ₁ , IndStrength ₂	0.96 \pm 0.02
All metrics	0.97 \pm 0.01

A.3. Extended results in multimodal experiments

A.3.1. ROPE CONTINUES TO RAISE THE DATA COMPLEXITY THRESHOLD FOR MULTIMODAL ICL.

Consistent with our unimodal results, Rope continues to raise the data complexity threshold for multimodal ICL to emerge, as shown in the Figure 13.

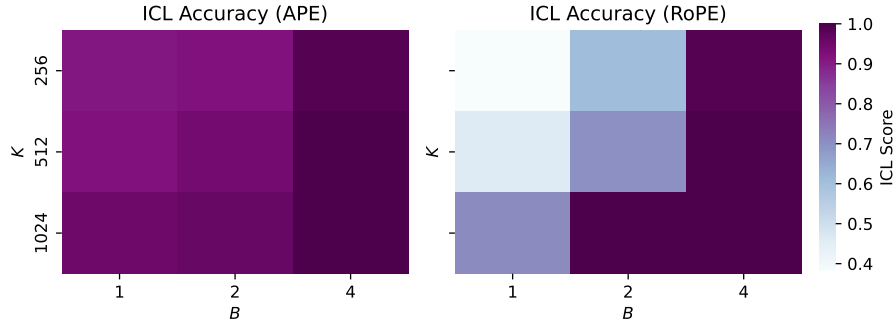


Figure 13. In the multimodal setting, RoPE yields lower ICL accuracy than APE across data regimes. Consistent with unimodal setting, RoPE increases the data complexity threshold for strong ICL.

A.3.2. IMPACT OF FEATURE DIMENSIONALITY ON CROSS-MODAL ALIGNMENT

To investigate the relationship between feature dimensionality and ICL performance, we measured the alignment between the projected M2 features and M1 class prototypes using Centered Kernel Alignment (CKA) and Euclidean Distance (L_2). The results are shown in the Table 6. As the feature dimension D_2 increases from 32 to 512, we observe a consistent degradation in alignment metrics: CKA values drop and L_2 distances increase (Row 1 vs. Row 4). While introducing the encoder consistently improves alignment compared to the “Projector Only” baseline (e.g., at $D_2 = 512$, CKA improves from 0.07 to 0.10 and L_2 decreases from 2.15 to 1.95), it does not fully restore the metrics to the levels observed at lower dimensions ($D_2 = 32$). This indicates that while the encoder mitigates misalignment, higher dimensionality introduces structural discrepancies that persist even with the encoder.

Table 6. Higher M2 feature dimensions(D_2) degrade alignment (CKA \downarrow , $L_2 \uparrow$). Here we use the feature after the projector for both with and without encoder settings. We fix $D_1 = 64$.

D_2	CKA w/o Enc	CKA w/ Enc	L_2 w/o Enc	L_2 w/ Enc
32	0.16	0.17	0.95	0.91
128	0.12	0.14	1.47	1.37
256	0.09	0.11	1.82	1.43
512	0.07	0.11	2.15	1.45

A.3.3. DATA DISTRIBUTIONAL FINDINGS TRANSFER TO REAL IMAGE DATA.

We extend our experiments on Omniglot dataset, which has 1.6k handwritten characters. We pre-train the decoder on GMM data and construct the multimodal input by varying the number of classes, the burstiness, within-class variance (adding noise), and the class distribution. The results in Figure 14 show that findings from the synthetic setting transfer.

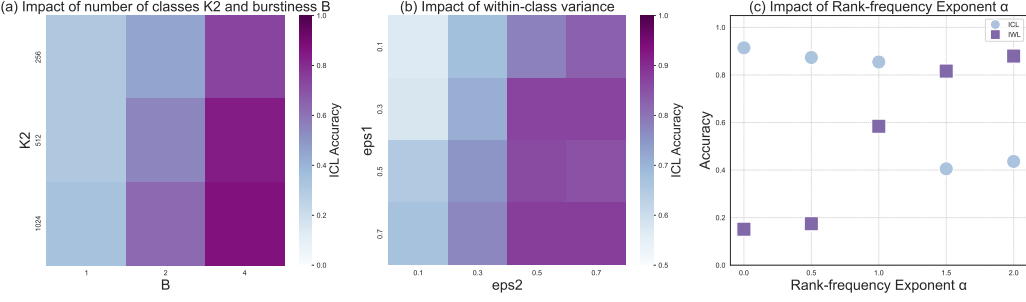


Figure 14. The data distributional findings transfer from the GMM setting to the **Omniglot** dataset. (a) Larger number of classes K_2 and burstiness B promotes ICL. The symmetry also transfers. When $K_1 = 8192$, a smaller $K_2 = 256$ is enough for the model to learn a very good ICL. (b) Within-class variation. Increasing ε_1 and ε_2 promotes ICL. (c) Class-distribution skew. Increasing α improves ICL. When $\alpha_1 = \alpha_2 = 1$, a balance is achieved between ICL and IWL.

A.3.4. HOW DOES THE PRETRAINING DATASET FOR THE ENCODER IMPACT DOWNSTREAM MULTIMODAL ICL?

We pretrain a family of encoders on Omniglot with controlled difficulty (class noise, sample count, label skew, regularization), yielding a range of validation accuracies. Each encoder is attached to the same projector and pretrained decoder, then fine-tuned under identical regimes. Encoder validation accuracy strongly predicts downstream multimodal ICL, whereas encoder size and the specific pretraining statistics do not show a clear independent effect (Figs. 15, 16).

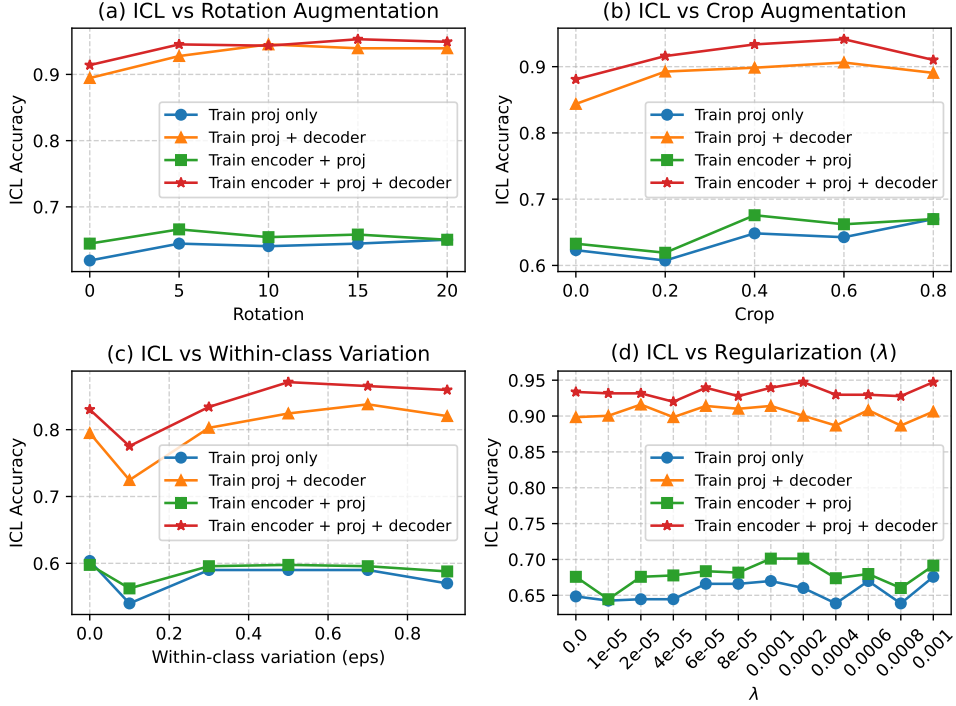


Figure 15. The correlation between statistical properties and regularization during encoder pretraining with the downstream ICL does not show a clear pattern across different training regimes.

A.3.5. PROGRESS MEASUREMENT ANALYSIS

Pearson Correlation. As shown in the Table 4b, PHStrength₁⁽¹⁾ shows weaker correlation with ICL compared with IndStrength₂. During the unimodal pretraining stage, the model already learns a strong previous-token head in the first layer which is retained in the multimodal stage, as shown in the Figure 9. It indicates that in the multimodal training stage, the dominant learning objective is to match the new modality to the correct class, making the continued development of the

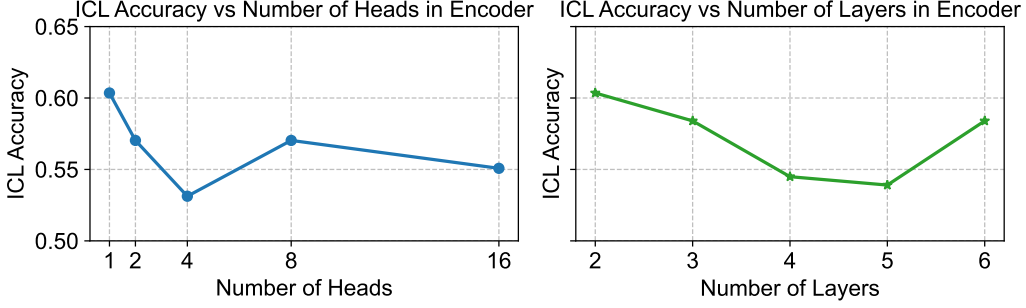


Figure 16. The encoder size shows no clear correlation with multimodal ICL accuracy.

induction head the most sensitive indicator of progress. Similarly, *CLA* exhibits a very low correlation with ICL accuracy because the model has learned in the first stage to predict the label from the context. In the multimodal training, *CLA* maintains at a very high value as shown in the Figure 9. *TLA*₁ continues to play a role as in the unimodal setting and interestingly, *TLA*₂ shows a moderately strong correlation with ICL accuracy ($r = 0.54$), but we find that it correlates even more strongly with *IndStrength*₂ ($r = 0.84$). This suggests that the predictive power of *TLA*₂ on ICL may be largely mediated through its alignment with *IndStrength*₂, which is the dominant indicator of ICL performance in this stage ($r = 0.68$). In this view, *TLA*₂ does not independently drive ICL, but rather co-develops with induction behavior. As the model learns to retrieve the correct label via contextual matching (induction), it also increases its attention to label positions more generally. This leads to a shared rise in both metrics, resulting in high intercorrelation and a secondary correlation with ICL. Thus, *TLA*₂’s relevance to ICL may be best understood as a supporting mechanism that reflects the formation of stronger induction behavior in the second layer.

Random forest prediction. The results in Table 7 confirm that the core induction mechanism remains the primary driver: using just *PHStrength*₁⁽¹⁾ and *IndStrength*₂ achieves a strong predictive performance with $R^2 = 0.9$. Adding *TLA*₁ improves the R^2 to 0.96. In contrast, adding *TLA*₂ results in a smaller gain ($R^2 = 0.92$), which supports our interpretation that its contribution is largely redundant with *IndStrength*₂. Using all available metrics yields $R^2 = 0.98$, showing that multimodal ICL accuracy can be predicted with high fidelity from a small set of interpretable attention behaviors.

Table 7. RF performance (R^2) using subsets of the progress measurements in the multimodal setting.

Feature subset	R^2 (mean \pm std)
<i>PHStrength</i> ₁ ⁽¹⁾ , <i>IndStrength</i> ₂	0.90 ± 0.01
<i>PHStrength</i> ₁ ⁽¹⁾ , <i>IndStrength</i> ₂ , <i>TLA</i> ₁	0.96 ± 0.06
<i>PHStrength</i> ₁ ⁽¹⁾ , <i>IndStrength</i> ₂ , <i>TLA</i> ₂	0.92 ± 0.01
All metrics	0.98 ± 0.01

A.3.6. CROSS-MODAL INTERACTION ANALYSIS VIA MODALITY ZEROING

To directly test whether the model performs genuine cross-modal reasoning or simply relies on a degenerate M1-only strategy, we conduct an ablation study where we selectively remove one modality at test time by replacing its tokens with zero vectors.

We take a model trained on multimodal sequences $x_1, x'_1, \ell_1, x_2, x'_2, \ell_2, \dots, x_q, x'_q$ and evaluate it under three conditions:

- **Full (M1 + M2):** standard evaluation with both modalities present
- **M1 only (M1 + zeros):** replace all M2 tokens x'_i with zero vectors
- **M2 only (zeros + M2):** replace all M1 tokens x_i with zero vectors

Table 8 shows that zeroing either modality substantially degrades ICL accuracy, confirming that the model relies on both modalities during inference. Zeroing M2 reduces accuracy to 0.336 (−65.2%), showing that removing the secondary

modality’s information substantially harms performance. Zeroing M1 is even more severe, reducing accuracy to 0.063 (−93.5%), which indicates that while the induction circuit was initially installed by M1 during pretraining, M2 alone cannot recover ICL without the primary modality’s contextual structure. These results, combined with our progress measurement analysis in Sec. 4.4.2, demonstrate that multimodal ICL is not a degenerate M1-only process. The model genuinely integrates information from both modalities through the shared self-attention mechanism.

Table 8. Modality ablation results. ICL accuracy drops dramatically when either modality is removed, confirming genuine cross-modal integration.

Input Type	M1 + M2	M1 + zeros	zeros + M2
ICL Accuracy	0.967	0.336	0.063

A.3.7. EARLY-FUSION JOINT TRAINING

In the main paper, we train the decoder on M1 (unimodal pretraining) before introducing M2 via a projector (late fusion). To understand how the observed modality asymmetry depends on this training schedule, we conducted additional experiments with **early-fusion joint training**, where both modalities are trained together from scratch.

We initialize a transformer from scratch and train it jointly on both M1 and M2. Since M1 and M2 have different dimensionalities ($D_1 \neq D_2$), we use a simple projector to map M2 into M1’s embedding space. The input sequence is $x_1, x'_1, \ell_1, x_2, x'_2, \ell_2, \dots, x_q, x'_q$, where x_i are M1 tokens and x'_i are projected M2 tokens. We systematically vary the number of classes in each modality (K_1, K_2) and the burstiness B , then measure ICL and IWL accuracies.

Tables 9 report the corresponding ICL and IWL accuracies. The results reveal a reversal of the asymmetry observed in late-fusion training. In late fusion, where M1 pretraining installs the induction circuit before M2 is introduced, varying K_1 has a stronger effect on ICL than varying K_2 . In early fusion, the opposite is true: varying K_2 shows a much stronger effect on ICL performance across all burstiness levels. This reversal is explained by the positional structure of the sequence. In our early-fusion setup, each label ℓ_i is positioned immediately after the M2 token x'_i rather than the M1 token x_i . Consequently, the simplest previous-token pattern the model can learn is to attend from ℓ_i to x'_i , and the simplest induction pattern for the query token is to locate the matching x'_i (in M2) and move one step forward to retrieve the label. This architectural design naturally encourages the induction circuit to anchor on M2. The primary-modality asymmetry observed in Sec. 4.1 is not a fixed property of the modalities themselves but emerges from the combination of pretraining schedule (which modality first learns the circuit) and sequence geometry (which tokens are positionally adjacent to labels). In late-fusion architectures with unimodal pretraining, the text modality becomes primary because it installs the induction circuit during language pretraining. Early-fusion joint training can shift this role to the vision modality if the sequence structure favors it.

Table 9. **Early fusion performance analysis.** A comparison of In-Context Learning (ICL) and In-Weights Learning (IWL) accuracy across varying number of classes (K_1, K_2) and burstiness (B).

$K_2 \setminus K_1$	$B = 1$				$B = 2$				$B = 4$			
	2048	4096	8192	16384	2048	4096	8192	16384	2048	4096	8192	16384
<i>In-Context Learning (ICL) Accuracy</i>												
2048	0.25	0.25	0.27	0.25	0.37	0.39	0.39	0.38	0.59	0.57	0.56	0.56
4096	0.28	0.26	0.25	0.26	0.37	0.39	0.37	0.35	0.57	0.58	0.59	0.56
8192	0.27	0.27	0.28	0.29	0.62	0.37	0.37	0.35	0.88	0.95	0.88	0.96
16384	0.26	0.27	0.29	0.31	0.52	0.65	0.50	0.57	0.89	0.87	0.58	0.88
<i>In-Weights Learning (IWL) Accuracy</i>												
2048	1.00	0.99	0.99	0.99	0.97	0.98	0.98	0.97	0.67	0.68	0.65	0.65
4096	0.98	0.97	0.97	0.98	0.70	0.70	0.73	0.73	0.46	0.41	0.38	0.43
8192	0.24	0.24	0.23	0.24	0.09	0.12	0.15	0.13	0.09	0.08	0.08	0.10
16384	0.10	0.10	0.10	0.09	0.09	0.08	0.08	0.09	0.07	0.07	0.09	0.08

A.4. Additional Evidence on Production MLLMs

We evaluate Qwen2.5-VL (3B, 7B) (Team, 2025) and IDEFICS (9B, 80B) (Laurençon et al., 2023) on VL-ICL benchmark, a suite designed to directly measure the ICL ability of vision–language models Zong et al. (2024). We then compute the strength of the previous token head and induction head for Qwen2.5-VL (3B, 7B) to investigate whether the controlled findings on the correlation between ICL accuracy and the strength of the induction circuits hold in MLLMs. The results reinforce two conclusions from our controlled experiments: (i) scaling the decoder improves multimodal ICL, and (ii) the positive correlation between the ICL accuracy and the strength of the induction circuit transfers to real models.

VL-ICL benchmark results. Table 10 shows that Qwen2.5-VL-7B consistently outperforms the 3B variant across all six tasks. The consistent direction of change across diverse task types supports the scalability of multimodal ICL. The IDEFICS family exhibits an even clearer scaling signal: moving from 9B to IDEFICS2-80B raises average accuracy by +10.52 %. Together, these results indicate that larger decoders yield stronger in-context learning in multimodal scenarios, not just in language-only settings.

Table 10. VL-ICL performance on production MLLMs. Accuracy (%) across six tasks comparing Qwen2.5-VL-3B/7B and IDEFICS-9B/IDEFICS2-80B. Both families improve with scale, supporting our finding that decoder scaling enhances multimodal ICL.

Task	Qwen2.5-VL-3B	Qwen2.5-VL-7B	IDEFICS-9B	IDEFICS-80B
CLEVR	5.50	7.50	30.33	32.43
Matching-MI	54.25	58.75	0.00	28.30
Open-MI	58.75	62.75	59.17	61.50
Operator Induction	8.35	8.50	14.44	21.67
Operator Induction (Interleaved)	10.00	11.35	15.00	36.67
TextOCR	46.50	48.50	28.00	29.50
Average	30.56	32.89 (+ 2.33 ↑)	24.49	35.01 (+ 10.52↑)

Circuit analysis and head measurements. We compute the strength of the previous token head and induction head for Qwen2.5-VL to identify the correlation between the induction circuit strength and ICL accuracy in the real MLLMs. For each attention head, we compute PHStrength(1) as the mean attention weight to the immediately preceding token and IndStrength as the attention that tokens place on positions right after any earlier occurrence of the same token—i.e., places where the model could copy from a matching in-context exemplar. Unlike Sec. 4.4, real MLLM inference doesn’t have a single “target query” token, so we aggregate and average this induction-directed attention across all tokens in the sequence, rather than measuring it at one designated query position. We evaluate these metrics on a batch of samples from the Open-MI task in the VL-ICL benchmark and rank heads by their average scores across samples. We show that scaling 3B→7B increases the ICL accuracy and also amplifies both components in the induction circuits: the strongest previous-token head increases from 0.105 to 0.127 (+20.8%), the strongest induction head from 0.009 to 0.011 (+25.3%); across the top-10, median gains are +2.3%(Prev) and +30.9% (Ind). These head-strength gains, especially IndStrength, track the VL-ICL accuracy improvements (Table 11).

Table 11. **Top-10 head strengths by rank, side-by-side.** Each entry shows the layer-head index (L, H) and strength s . “PHStrength⁽¹⁾” = previous-token behavior; “IndStrength” = induction behavior. The relative change is $\Delta\% = 100 \times \frac{s_{7B} - s_{3B}}{s_{3B}}$, so positive values mean the 7B head is stronger than the 3B head.

Rank	PHStrength ⁽¹⁾			IndStrength		
	Qwen-3B (L,H; s)	Qwen-7B (L,H; s)	$\Delta\%$	Qwen-3B (L,H; s)	Qwen-7B (L,H; s)	$\Delta\%$
1	(19,11; 0.1047)	(13,13; 0.1265)	+20.8	(17,10; 0.0091)	(15,20; 0.0114)	+25.3
2	(19, 1; 0.0738)	(15,11; 0.0626)	-15.2	(5, 9; 0.0073)	(8,22; 0.0106)	+45.2
3	(31, 9; 0.0623)	(1,15; 0.0570)	-8.5	(5,14; 0.0060)	(4, 9; 0.0088)	+46.7
4	(1, 1; 0.0582)	(10,22; 0.0530)	-8.9	(3, 6; 0.0059)	(4,11; 0.0087)	+47.5
5	(19, 5; 0.0516)	(0, 6; 0.0527)	+2.1	(31,10; 0.0054)	(16, 9; 0.0086)	+59.3
6	(2,13; 0.0491)	(15, 5; 0.0505)	+2.9	(22,14; 0.0054)	(15,19; 0.0071)	+31.5
7	(24,15; 0.0461)	(11,19; 0.0472)	+2.4	(3,13; 0.0049)	(8,24; 0.0059)	+20.4
8	(15, 9; 0.0456)	(21,15; 0.0470)	+3.1	(6, 6; 0.0048)	(2,22; 0.0057)	+18.8
9	(18,11; 0.0450)	(3,10; 0.0452)	+0.4	(17,11; 0.0043)	(3,11; 0.0056)	+30.2
10	(18,15; 0.0419)	(3,24; 0.0449)	+7.2	(6, 9; 0.0043)	(27,13; 0.0050)	+16.3
Median $\Delta\%$		+2.3\uparrow		+30.9\uparrow		